

## HUMAN GRASPING FORCE PREDICTION, MEASUREMENT, AND VALIDATION FOR HUMAN-ROBOT LIFTING

**Asif Arefeen**

Mechanical and Aerospace Engineering  
Oklahoma State University  
Stillwater, Oklahoma 74078, USA

**Joel Quarnstrom**

Mechanical and Aerospace Engineering  
Oklahoma State University  
Stillwater, Oklahoma 74078, USA

**Shahbaz P Qadri Syed**

Mechanical and Aerospace Engineering  
Oklahoma State University  
Stillwater, Oklahoma 74078, USA

**He Bai**

Mechanical and Aerospace Engineering  
Oklahoma State University  
Stillwater, Oklahoma 74078, USA

**Yujiang Xiang<sup>1</sup>**

Mechanical and Aerospace Engineering  
Oklahoma State University  
Stillwater, Oklahoma 74078, USA

### ABSTRACT

*In this study, a 13 degrees of freedom (DOFs) three-dimensional (3D) human arm model and a 10 DOFs 3D robotic arm model are used to validate the grasping force for human-robot lifting motion prediction. The human arm and robotic arm are modeled in Denavit-Hartenberg (DH) representation. In addition, the 3D box is modeled as a floating-base rigid body with 6 global DOFs. The human-box and robot-box interactions are characterized as a collection of grasping forces. The joint torque squares of human arm and robot arm are minimized subjected to physics and task constraints. The design variables include (1) control points of cubic B-splines of joint angle profiles of the human arm, robotic arm, and box; and (2) the discretized grasping forces during lifting. Both numerical and experimental human-robot liftings were performed with a 2 kg box. The simulation reports the human arm's joint angle profiles, joint torque profiles, and grasping force profiles. The comparisons of the joint angle profiles and grasping force profiles between experiment and simulation are presented. The simulated joint angle profiles have similar trends to the experimental data. It is concluded that human and robot share the load during lifting process, and the predicted human grasping force matches the measured experimental grasping force reasonably well.*

Keywords: Motion planning, human-robot interaction, force sensors, sawyer robot, and inverse dynamic optimization.

### 1. INTRODUCTION

Human-robot collaboration is a topic of study with a wide range of applications and a significant economic impact.

Collaboration between humans and robots can significantly accelerate production processes, enhance manufacturing quality, and lower structural costs. However, it is necessary to predict the human-robot lifting motion with grasping forces to avoid any human injuries.

Researchers have developed various biomechanical prediction models for lifting over the previous few decades [1-6]. Furthermore, human-robot interaction research has made great progress. Different learning techniques are currently being used by researchers to anticipate and execute lifting tasks successfully. Evrard et al. [7] presented a probabilistic framework for conducting a human-robot collaborative task with the help of a human operator. DelPreto and Rus [8] used EMG signals to estimate the human's intention in a real-time interface for controlling collaborative object lifting tasks. Calinon et al. [9] studied a robotic learning system to reproduce collaborative lifting with a haptic interface. Xiang and Arefeen [4] developed a human-human collaborative lifting motion prediction with grasping forces. In addition, an optimization-based human-robot collaborative lifting motion prediction has been developed in previous research [10].

This work extends our previous collaborative lifting prediction for the 3D and 2D skeleton models [4, 10]. This study aims to predict, measure, and validate the grasping force for human-robot lifting motion prediction. To predict the collaborative lifting motion and hand grasping forces, an inverse dynamics optimization formulation is proposed. A nonlinear programming (NLP) optimization problem is used to address the human-robot lifting problem. The objective function is the sum of human and robot joint torques squared, which is minimized using the SQP algorithm [11]. The optimization and

<sup>1</sup> Corresponding author: yujiang.xiang@okstate.edu

experimental results are presented, and a valid comparison is established.

## 2. METHOD

### 2.1 Human-robot system

This study takes into account a 13 DOF 3D human skeleton arm model and a 10 DOF robotic arm model. A floating-base rigid box with 6 DOF is also utilized for lifting, as illustrated in Figure 1. The DH approach was used to construct all models [12]. Furthermore, two grasping force vectors ( $\mathbf{f}_1^c$  and  $\mathbf{f}_2^c$ ) act on the box's two bottom edges. The equations of motion (EOM) of human, robot, and box systems are set up using the recursive Lagrangian dynamics formulation [4, 13]. The system's dynamics equation can be written as:

$$\tau_i = \text{tr} \left( \frac{\partial \mathbf{A}_i}{\partial q_i} \mathbf{D}_i \right) - \mathbf{g}^T \frac{\partial \mathbf{A}_i}{\partial q_i} \mathbf{E}_i - \mathbf{f}_k^T \frac{\partial \mathbf{A}_i}{\partial q_i} \mathbf{F}_i - \mathbf{G}_i^T \mathbf{A}_{i-1} \mathbf{z}_0 \quad (1)$$

where the first term is inertia and Coriolis torque, the second term is the torque due to gravity, the third term is the torque due to external forces, and the fourth term is the torque due to external moments in equation (1). Here,  $\mathbf{f}_k = [f_{kx} \ f_{ky} \ f_{kz} \ 0]^T$  is the external force applied on link  $k$ , and details refer to [4].

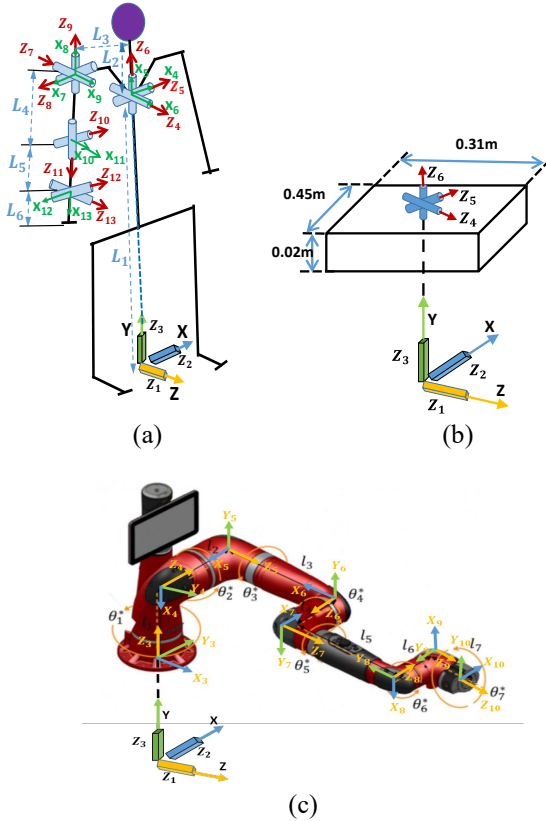


FIGURE 1: (a) THE 3D HUMAN SKELETAL ARM MODEL, (b) 3D BOX MODEL, AND (c) SAWYER ROBOTIC ARM

### 2.2 External forces as design variables

External forces can be expressed in equation (1) as fixed or variable quantities. This study treats the grasping external forces between the human and the box as unknowns (design variables). As a result, the EOM's joint torques are a function of both state variables  $\mathbf{q}$  and varying external forces (grasping forces). In order to use gradient-based optimization, the sensitivity of joint torque with respect to external force are determined. The joint torques are affected by the external load in the vertical direction  $f_{ky}$  in two ways: explicitly ( $\tau_i^o$ ) through the EOM and implicitly ( $\tau_i^{\sim}$ ) through the passive ground reaction forces (GRF). The differentiation of  $\tau_i^o$  with respect to  $f_{ky}$  can be calculated directly from the third term on the RHS of equation (1) as:

$$\frac{\partial \tau_i^o}{\partial f_{ky}} = [0 \ 1 \ 0 \ 0] \frac{\partial \mathbf{A}_i}{\partial q_i} \mathbf{F}_i \quad (2)$$

Furthermore, the GRF is derived using an active-passive algorithm [4] from human global joint torques, as shown in Figure 2.

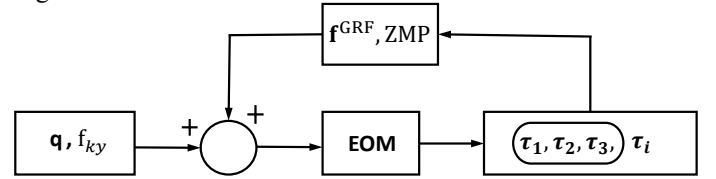


FIGURE 2: ACTIVE-PASSIVE (GRF) FEEDBACK

Here,  $\mathbf{f}^{GRF} = [f_x^{GRF}(\tau_{1\sim3}^o), f_y^{GRF}(\tau_{1\sim3}^o), f_z^{GRF}(\tau_{1\sim3}^o), 0]^T$  is defined as a function of  $\tau_{1\sim3}^o$  (active global joint torques). The chain rule is then used to compute the sensitivity of joint torque  $\tau_i^{\sim}$  with respect to  $f_{ky}$  due to GRF:

$$\frac{\partial \tau_i^{\sim}}{\partial f_{ky}} = \frac{\partial \tau_i^{\sim}}{\partial f_x^{GRF}} \frac{\partial f_x^{GRF}}{\partial \tau_{1\sim3}^o} \frac{\partial \tau_{1\sim3}^o}{\partial f_{ky}} + \frac{\partial \tau_i^{\sim}}{\partial f_y^{GRF}} \frac{\partial f_y^{GRF}}{\partial \tau_{1\sim3}^o} \frac{\partial \tau_{1\sim3}^o}{\partial f_{ky}} + \frac{\partial \tau_i^{\sim}}{\partial f_z^{GRF}} \frac{\partial f_z^{GRF}}{\partial \tau_{1\sim3}^o} \frac{\partial \tau_{1\sim3}^o}{\partial f_{ky}} \quad (3)$$

$$\frac{\partial \tau_i^{\sim}}{\partial f_x^{GRF}} = [1 \ 0 \ 0 \ 0] \frac{\partial \mathbf{A}_i}{\partial q_i} \mathbf{F}_i \quad (4)$$

$$\frac{\partial \tau_i^{\sim}}{\partial f_y^{GRF}} = [0 \ 1 \ 0 \ 0] \frac{\partial \mathbf{A}_i}{\partial q_i} \mathbf{F}_i \quad (5)$$

$$\frac{\partial \tau_i^{\sim}}{\partial f_z^{GRF}} = [0 \ 0 \ 1 \ 0] \frac{\partial \mathbf{A}_i}{\partial q_i} \mathbf{F}_i \quad (6)$$

Finally, the sum of equations (2) and (3) gives the sensitivity of the joint torque with respect to the active external load  $f_{ky}$ .

$$\frac{\partial \tau_i}{\partial f_{ky}} = \frac{\partial \tau_i^o}{\partial f_{ky}} + \frac{\partial \tau_i^{\sim}}{\partial f_{ky}} \quad (7)$$

Similarly, the external loads  $f_{kx}$  and  $f_{kz}$  sensitivity can be computed as follows:

$$\frac{\partial \tau_i}{\partial f_{kx}} = \frac{\partial \tau_i^o}{\partial f_{kx}} + \frac{\partial \tau_i^{\sim}}{\partial f_{kx}} \quad (8)$$

$$\frac{\partial \tau_i}{\partial f_{kz}} = \frac{\partial \tau_i^o}{\partial f_{kz}} + \frac{\partial \tau_i^{\sim}}{\partial f_{kz}} \quad (9)$$

## 2.3 Human-robot lifting experiment

The IRB-approved collaborative human-robot lifting study was conducted at Oklahoma State University with a single healthy male. OptiTrack motion capture (MOCAP) was used to obtain 3D kinematic data at 120 Hz. The room was surrounded by twelve prime 13W cameras. The subject was instructed to lift a 2 kg box with the robot collaboratively for the lifting task. The data was processed using the motion capture software Motive 2.2 after the experiment. The data were smoothed and transformed into a C3D file after all markers were labeled. After that, the C3D file was imported into Visual 3D. (C-Motion, Inc.). Following the marker protocol used in the experiments, a skeleton model was built. Coordinates, joint angles, and joint moments were generated using this skeleton model. The subject's anthropometric data were used to generate separate and accurate skeletal models, which enabled more precise calculations.

The human hand grasping force was collected using force sensitive resistor (FSR) pads. These FSRs were attached to the lifting weight (box) (Figure 3). This weight was a wooden board. There were four sensors on the bottom of the box and two on the top. A metal plate was attached to each set on the top and bottom to distribute the force evenly between FSRs. The human grips the board with their thumb contacting the top set of sensors, and their other four fingers contacting the bottom set of sensors. The resistance of each FSR was measured using a voltage divider circuit connected to an Arduino. The Arduino was controlled by a desktop computer running a MATLAB data acquisition system through a wired connection. The red arrows in Figure 3 represent the location of the force vectors of the human's fingers.

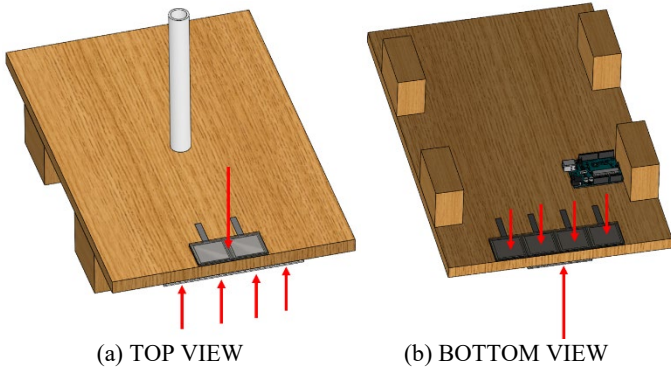


FIGURE 3: LIFTING BOX

The data collected by the Arduino was a voltage difference curve for each sensor over time. In order to determine the force corresponding to the detected voltages, the sensors were calibrated. A sensor was placed on a scale and incrementally loaded. The voltage and scale weight values were recorded. This calibration process was performed four times, and a spline curve was fit to this data. The spline served as a correlation between the recorded voltage and the actual force. A period of time was recorded for the sensors to determine if there was a voltage offset when they were unloaded. This value for each sensor was

subtracted from the recorded data to correct for preloading in the system.

A graphical user interface (GUI) was coded in MATLAB to start and stop the data recording and plot the sensor data as it was being collected (Figure 4). After the experiment, the force from the top resistors was summed to get the force applied by the thumb, and the sum of the force of the bottom resistors determined the force applied by the four fingers. The four-finger force minus the thumb force determined the total experimental hand reaction (grasping) force.

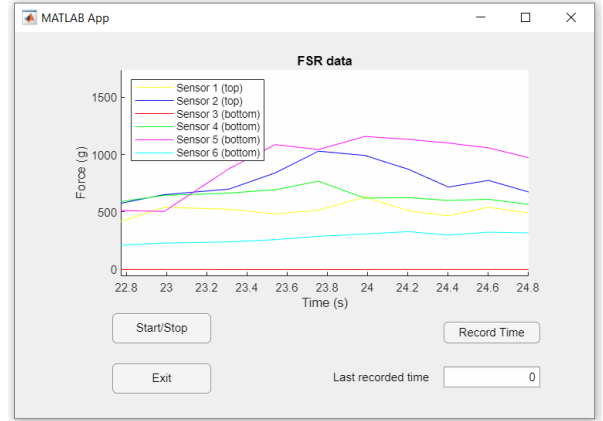


FIGURE 4: DATA COLLECTION GUI

## 3. OPTIMIZATION FORMULATION

### 3.1 Design variables

The design variables ( $\mathbf{x}$ ) are joint angle control points  $\mathbf{P}_{human}$ ,  $\mathbf{P}_{robot}$ , and  $\mathbf{P}_{box}$  for human, robot, and the box, since the joint angle profiles are discretized by cubic B-splines. Furthermore, the grasping forces ( $\mathbf{f}_1^c$  and  $\mathbf{f}_2^c$ ) between human and box, and robot and box, are treated as additional design variables. So,  $\mathbf{x} = [\mathbf{P}_{human}^T, \mathbf{P}_{robot}^T, \mathbf{P}_{box}^T, \mathbf{f}_1^{cT}, \mathbf{f}_2^{cT}]^T$ .

### 3.2 Objective functions

The objective function is the sum of joint torque squares for human and robot [4, 10].

$$J(\mathbf{x}) = w_1 \sum_{i=6}^{n_{human}} \int_0^T \{\tau_{i(human)}^2(\mathbf{P}_{human}, \mathbf{f}_1^c)\} dt + w_2 \sum_{i=3}^{n_{robot}} \int_0^T \{\tau_{i(robot)}^2(\mathbf{P}_{robot}, \mathbf{f}_2^c)\} dt \quad (10)$$

where  $n_{human} = 13$ ,  $n_{robot} = 10$ , and  $T$  is the total time. The total time duration  $T$  is a specified input parameter,  $w_1$  and  $w_2$  are weighting coefficients for human and robot performance measure, respectively.

### 3.3 Constraints

The basic constraints include (1) joint angle limits, (2) torque limits, (3) feet/base contacting position, (4) box forward,

(5) box range of motion, (6) box grasping, (7) box global EOM, (8) initial and final box locations, and (9) static conditions at the start and end of the motion. Constraints (1-4) apply to both the human and the robot, while constraints (5-7) only apply to the box. The box grasping and box global EOM constraints are expressed in the following equations:

$$p_{human\_wrist}(t) - p_{box}^L(t) = 0 \quad (11)$$

$$p_{robot\_end\_effector}(t) - p_{box}^R(t) = 0 \quad (12)$$

$$|\tau_i^{box}| \leq \varepsilon, \quad i = 1, 2, 3, 4, 5, 6 \quad (13)$$

where  $p_{human\_wrist}$  and  $p_{robot\_end\_effector}$  are the wrist and end-effector positions of the human and robot arm, respectively.  $p_{box}^L$  and  $p_{box}^R$  are the left and right edge positions of the box. Furthermore,  $\tau_{box}$  is the global joint force and torque values of the box,  $\varepsilon = 1$  N. Two external grasping forces are acting on the box edges to keep it in balance. Detail formulations of all the constraints are referred to [4].

#### 4. RESULTS

The NLP problem for human-robot lifting is solved using an SQP method in SNOPT [11]. The initial guess for the optimization are  $\mathbf{P} = [\mathbf{P}_{human}, \mathbf{P}_{robot}, \mathbf{P}_{box}] = \mathbf{0}$ ,  $\mathbf{f}_1^c = \mathbf{f}_2^c = \mathbf{10}$ . There are total 224 design variables and 898 nonlinear constraints. The optimal solution is obtained in 15.93 seconds on a laptop with an Intel® Core™ i7 2.11 GHz CPU and 16 GB RAM. The collaborative box-lifting task required input data such as box weight of 2 kg, total time of 2.0 seconds, and initial and final box locations.

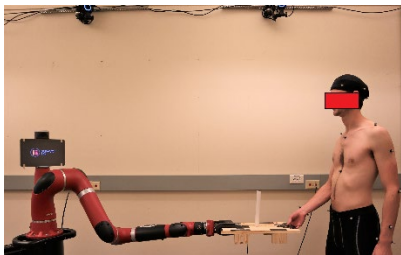
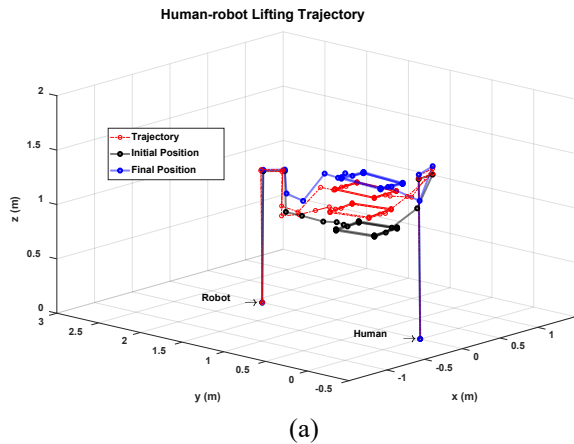


FIGURE 5: (a) SIMULATION SNAPSHOTS AND (b) EXPERIMENT FOR HUMAN-ROBOT LIFTING

First, Figure 5 illustrates a snapshot of the predicted 3D human-robot arm lifting motion from the simulation and the experimental scenario. Figure 6 presents a comparison of experimental and simulation joint angles for human shoulder flexion and elbow flexion. Furthermore, the joint torque profiles for human shoulder flexion, and elbow flexion are shown in Figure 7. Finally, human box grasping forces comparisons are presented in Figure 8.

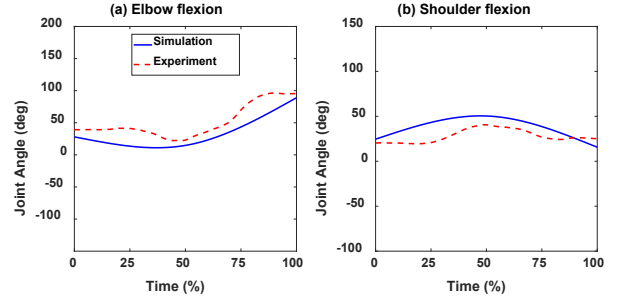


FIGURE 6: HUMAN ARM JOINT ANGLE PROFILES COMPARISON BETWEEN SIMULATION AND EXPERIMENT

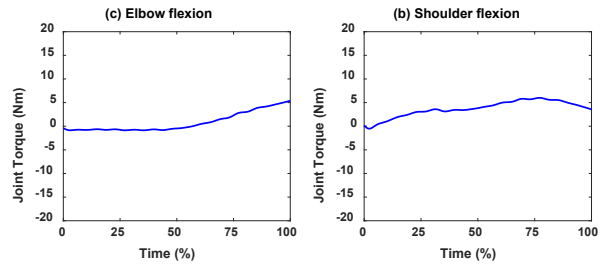


FIGURE 7: HUMAN ARM JOINT TORQUE PROFILES

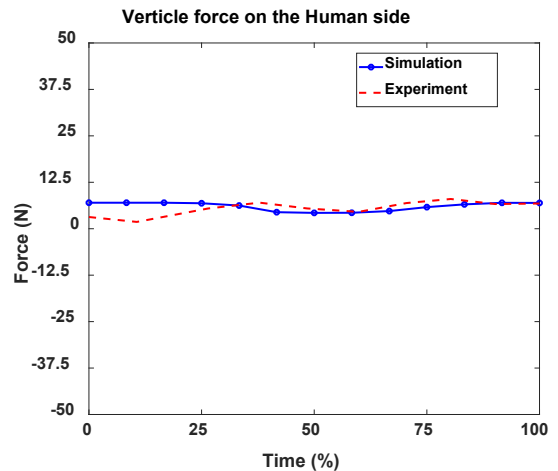


FIGURE 8: HUMAN BOX GRASPING FORCE COMPARISON BETWEEN SIMULATION AND EXPERIMENT

## 5. DISCUSSION

The trajectory of the simulated human-robot lifting motion and the human-robot initial position in the experiment are depicted in Figure 5. In this study, the initial and final box locations are symmetric, and the optimization predicts a natural collaborative lifting motion. In Figure 6, the experimental elbow flexion joint angle profile is larger than the simulated joint angle profile. The experimental shoulder flexion joint angle is less than the simulated joint angle. Both the simulated and experimental joint angle profiles show similar trends. The lifting approach may differ from subject to subject, and it is quite difficult to follow the simulation results precisely in a real-world scenario. Furthermore, when the joint angle increases, so does the magnitude of the simulated joint torque profile of elbow flexion. In the same way, the magnitude of the joint torque profile of shoulder flexion follows the joint angle trend, as illustrated in Figure 7.

In the comparison of human box grasping forces, the experimental vertical grasping force on the human side is initially lower than the simulated force. The experimental force, however, follows the simulated grasping force after the first 25% of the overall lifting duration. Five force sensors were utilized in the experiment, and it is anticipated that naturally, the human did not press the sensors adequately at first. But, after a while (25%) the human adapted to the robot motion during the lifting process.

## 6. CONCLUSION

In this study, the lifting motion and grasping forces of human-robot were predicted using an inverse dynamics optimization formulation. SNOPT, a gradient-based optimizer, effectively solved the NLP optimization problems. Simulation results were found to be reasonable. The simulation results are compared to the experimental data that include joint angle profiles from motion capture and hand grasping force profiles from force sensors. The proposed grasping force optimization formulation can be used to design the best human-robot collaborative lifting to prevent human injury. The next goal is to establish a lifting database, we will conduct the experiments and simulations with different subjects and varying box weights [14] in the future.

## ACKNOWLEDGEMENTS

This study is partially supported by Grant No. T42OH008421 from the NIOSH / CDC to the Southwest Center for Occupational and Environmental Health (SWCOEH), NSF project CBET 1849279, and Research Jumpstart/Accelerator Grant from Oklahoma State University.

## REFERENCES

[1] Xiang, Y., Arora, J.S., Rahmatalla, S., Marler, T., Bhatt, R., Abdel-Malek, K., 2010, Human lifting simulation using a multi-objective optimization approach, *Multibody System Dynamics*, 23(4), 431-451.

[2] Xiang, Y., Arora, J.S., & Abdel-Malek, K. 2012, 3D human lifting motion prediction with different performance measures. *International Journal of Humanoid Robotics*, 9(02), 1250012.

[3] Song, J., Qu, X., & Chen, C.H., 2016, Simulation of lifting motions using a novel multi-objective optimization approach. *International Journal of Industrial Ergonomics*, 53, 37-47.

[4] Xiang, Y., Arefeen, A., 2020, Two-dimensional team lifting prediction with floating-base box dynamics and grasping force coupling. *Multibody System Dynamics*, 50, 211–231.

[5] Wang, Q., Xiang, Y., Kim, H.J., Arora, J.S., Abdel-Malek, K., 2005. Alternative formulations for optimization-based digital human motion prediction. *Proceedings of 2005 Digital Human Modeling for Design and Engineering Symposium*, Iowa City, IA.

[6] Xiang, Y., Zaman, R., Rakshit, R., and, Yang, J., 2019, Subject-specific strength percentile determination for two-dimensional symmetric lifting considering dynamic joint strength. *Multibody System Dynamics*, 46(1), 63-76.

[7] Evrard, P., Gribovskaya, E., Calinon, S., Billard, A., and Kheddar, A., 2009, Teaching physical collaborative tasks: object-lifting case study with a humanoid. *2009 9th IEEE-RAS International Conference on Humanoid Robots*, Paris, France, pp. 399-404, doi: 10.1109/ICHR.2009.5379513.

[8] DelPreto, J., and Rus, D., 2019, Sharing the load: human-robot team lifting using muscle activity. In: *2019 IEEE International Conference on Robotics and Automation (ICRA)*, May 20-24, Montreal, Canada.

[9] Calinon, S., Evrard, P., Gribovskaya, E., Billard, A. and Kheddar, A., 2009, Learning collaborative manipulation tasks by demonstration using a haptic interface. In: *2009 International Conference on Advanced Robotics*, pp.1-6.

[10] Arefeen, A., Xiang, Y., 2021, Design human-robot collaborative lifting task using optimization. *Proceedings of the ASME 2021 International Design Engineering Technical Conferences and Computers and Information in Engineering Conference*, August 17–19, 2021, online, V002T02A010, ASME.

[11] Gill, P.E., Murray, W., and Saunders, M.A., 2002, SNOPT: An SQP algorithm for large-scale constrained optimization. *SIAM Journal of Optimization*, 12(4), 979-1006.

[12] Denavit, J., and Hartenberg, R.S., 1955, A kinematic notation for lower-pair mechanisms based on matrices. *Journal of Applied Mechanics*, 22, 215-221.

[13] Xiang, Y., Arora, J.S., Rahmatalla, S., Abdel-Malek, K., 2009. Optimization-based dynamic human walking prediction: one step formulation. *International Journal for Numerical Methods in Engineering*, 79(6), 667-695.

[14] Arefeen, A., Xiang, Y., 2020, Two-dimensional team lifting prediction with different box weights. *Proceedings of the ASME 2020 International Design Engineering Technical Conferences and Computers and Information in Engineering Conference*. August 17–19, 2020, Online, V009T09A004. ASME.